© 2017. Published by The Company of Biologists Ltd | Journal of Cell Science (2017) 130, 1772-1784 doi:10.1242/jcs.201103

RESEARCH ARTICLE

Multiple roles of integrin-α3 at the neuromuscular junction

Jacob A. Ross[1,*], Richard G. Webster[2], Tanguy Lechertier[3], Louise E. Reynolds[3], Mark Turmaine[4], Maximilien Bencze[1], Yalda Jamshidi[5], Hakan Cetin[2], Francesco Muntoni[1], David Beeson[2], Kairbaan Hodilvala-Dilke[3] and Francesco J. Conti[1,‡]

ABSTRACT

The neuromuscular junction (NMJ) is the synapse between motoneurons and skeletal muscle, and is responsible for eliciting muscle contraction. Neurotransmission at synapses depends on the release of synaptic vesicles at sites called active zones (AZs). Various proteins of the extracellular matrix are crucial for NMJ development; however, little is known about the identity and functions of the receptors that mediate their effects. Using genetically modified mice, we find that integrin-α3 (encoded by *Itga3*), an adhesion receptor at the presynaptic membrane, is involved in the localisation of AZ components and efficient synaptic vesicle release. Integrin-α3 also regulates integrity of the synapse – mutant NMJs present with progressive structural changes and upregulated autophagy, features commonly observed during ageing and in models of neurodegeneration. Unexpectedly, we find instances of nerve terminal detachment from the muscle fibre; to our knowledge, this is the first report of a receptor that is required for the physical anchorage of pre- and postsynaptic elements at the NMJ. These results demonstrate multiple roles of integrin-α3 at the NMJ, and suggest that alterations in its function could underlie defects that occur in neurodegeneration or ageing.

KEY WORDS: Adhesion receptor, Synapse, Autophagy, Neurodegeneration, Ageing

INTRODUCTION

The neuromuscular junction (NMJ) is the chemical synapse that exists between a motoneuron and a skeletal muscle fibre. Action potentials propagating along the axon reach the nerve terminal, triggering the release of the neurotransmitter acetylcholine (ACh). This binds to postsynaptic acetylcholine receptors (AChRs) on the muscle membrane, stimulating muscle contraction. Active zones (AZs) are essential for neurotransmitter release (Meriney and Dittrich, 2013; Südhof, 2012). On the arrival of an action potential, voltage-gated Ca^{2+} channels (VGCCs) in the AZs open, resulting in local influx of Ca^{2+}, fusion of synaptic vesicles with the presynaptic membrane and release of neurotransmitter into the synaptic cleft.

[1]Dubowitz Neuromuscular Centre, Institute of Child Health, University College London, 30 Guilford Street, London WC1N 1EH, UK. [2]Nuffield Department of Clinical Neurosciences, University of Oxford, John Radcliffe Hospital, Oxford OX3 9DS, UK. [3]Centre for Tumour Biology, Barts Cancer Institute, Queen Mary University of London, Charterhouse Square, London EC1M 6BQ, UK. [4]Department of Cell and Developmental Biology, University College London, Gower Street, London WC1E 6BT, UK. [5]Department of Genetics, Institute of Molecular and Clinical Sciences, St George's University of London, Cranmer Terrace, London SW17 0RE, UK.
*Present address: Centre of Human and Aerospace Physiological Sciences, Guy's Campus, King's College, London SE1 1UL, UK.

‡Author for correspondence (f.conti@ucl.ac.uk)

F.J.C., 0000-0002-9887-7323

Received 30 December 2016; Accepted 31 March 2017

The mechanisms leading to the formation of the presynaptic terminus at the NMJ are only partially understood, although various factors have been implicated, including growth factors and postsynaptic proteins acting as retrograde signals (Lrp4, MuSK) (Fox et al., 2007; Yumoto et al., 2012). The subsequent formation of the AZs depends on cues provided by the synaptic basal lamina, a layer of extracellular matrix (ECM) that occupies the synaptic cleft (Singhal and Martin, 2011). A key component of this is laminin-β2 (encoded by *Lamb2*), which combines with other subunits to form laminin-α2β2γ1, α4β2γ1 and α5β2γ1 (also known as laminin-221, -421 and -521, respectively). The laminin-β2 chain interacts with VGCCs on the presynaptic terminus, initiating AZ assembly (Chen et al., 2011; Nishimune et al., 2004). In addition to its functions in AZ assembly, the basal lamina is important for postsynaptic differentiation and maturation of the NMJ (Singhal and Martin, 2011).

Integrins are a family of heterodimeric cell surface receptors, consisting of an α and β subunit. They are central mediators of mechanotransduction, basal lamina organisation and signalling between intra- and extracellular compartments (Hynes, 2002). Integrin-β1 (encoded by *Itgb1*) is expressed both in muscle and in motoneurons. In mice, targeted knockout of integrin-β1 (disrupting the formation of all heterodimers containing integrin-β1) in muscle leads to severe defects in innervation, while surprisingly, knockout of integrin-β1 in motoneurons causes no obvious abnormalities (Schwander et al., 2004). Thus, integrins play important roles at the NMJ, but the function of specific subunits, particularly in mammals and in postnatal life, have remained elusive.

The integrin-α3β1 heterodimer is a laminin receptor found at the presynaptic AZs of the frog NMJ (Cohen et al., 2000), and of the *Torpedo* electric synapse (a model synapse with structural and molecular homology to the NMJ) (Carlson et al., 2010). In the latter, the heterodimer has been shown to complex with VGCCs and presynaptic cytoskeletal components, and with laminin-α4 in the synaptic cleft. We thus hypothesised that it may mediate some of the effects of the basal lamina at the NMJ. To investigate the roles of integrin-α3 at the NMJ, we analysed genetically modified mice with an ablation of the *Itga3* gene (Kreidberg et al., 1996). Integrin-α3 has crucial functions in mediating adhesion to the extracellular matrix (ECM), and genetic ablation leads to defects in skin, kidney and lung, with death shortly after birth. Using these mice, and also heterozygotes, which survive after birth, we demonstrate that integrin-α3 plays a role in the localisation of AZ components and synaptic vesicle release at the NMJ. In addition, the NMJs of heterozygous mice progressively accumulate morphological features that are found in aged (~2 year old) wild-type (WT) animals, and in a number of mouse models with neurodegeneration or NMJ defects, suggesting a role in synaptic maintenance (Fox et al., 2007, 2008; Latvanlehto et al., 2010; Samuel et al., 2012). Surprisingly, we also observed instances of localised detachment of presynaptic terminals from the basal lamina, suggesting that integrin-α3 mediates anchorage of the pre- and postsynaptic elements at the NMJ. These results reveal novel

Journal of Cell Science

Journal of Cell Science (2017) 130, 1772-1784 doi:10.1242/jcs.201103

roles for integrin-α3 in the formation of presynaptic apparatus and in the structural maintenance of the NMJ. Although adult mice heterozygous for integrin-α3 have no overt phenotype, the data suggest that defects or changes in integrin function could be associated with neurodegeneration or with normal ageing at the NMJ.

RESULTS

Integrin-α3 is concentrated at the AZs of NMJs and regulates their composition

To determine the localisation of integrin-α3 at the mouse NMJ, we stained longitudinal sections of sternomastoid muscle from embryonic day (E)18.5 mice with antibodies to integrin-α3 and with fluorescently conjugated α-bungarotoxin to mark postsynaptic AChR clusters (Fig. 1). We found a clear localisation of integrin-α3 apposed to the AChR plaque (Fig. 1A). Imaging at high magnification revealed that integrin-α3 was specifically concentrated at AZs, colocalizing with bassoon-positive puncta (Fig. 1B); this was verified using line scans across the synapse to measure fluorescence intensities and spatial distribution of integrin-α3, bassoon and AChRs (Fig. 1E). Loss of integrin-α3 was confirmed at the NMJs of the integrin-$\alpha3^{-/-}$ mouse (Fig. 1D) and, in addition, expression of the protein was markedly reduced in integrin-$\alpha3^{+/-}$ littermates (Fig. 1C,F; 48% reduction). With these results in mind, we decided to study further the NMJs of both integrin-$\alpha3^{+/-}$ and integrin-$\alpha3^{-/-}$ mice, to assess the consequences of partial (~50%) or complete ablation.

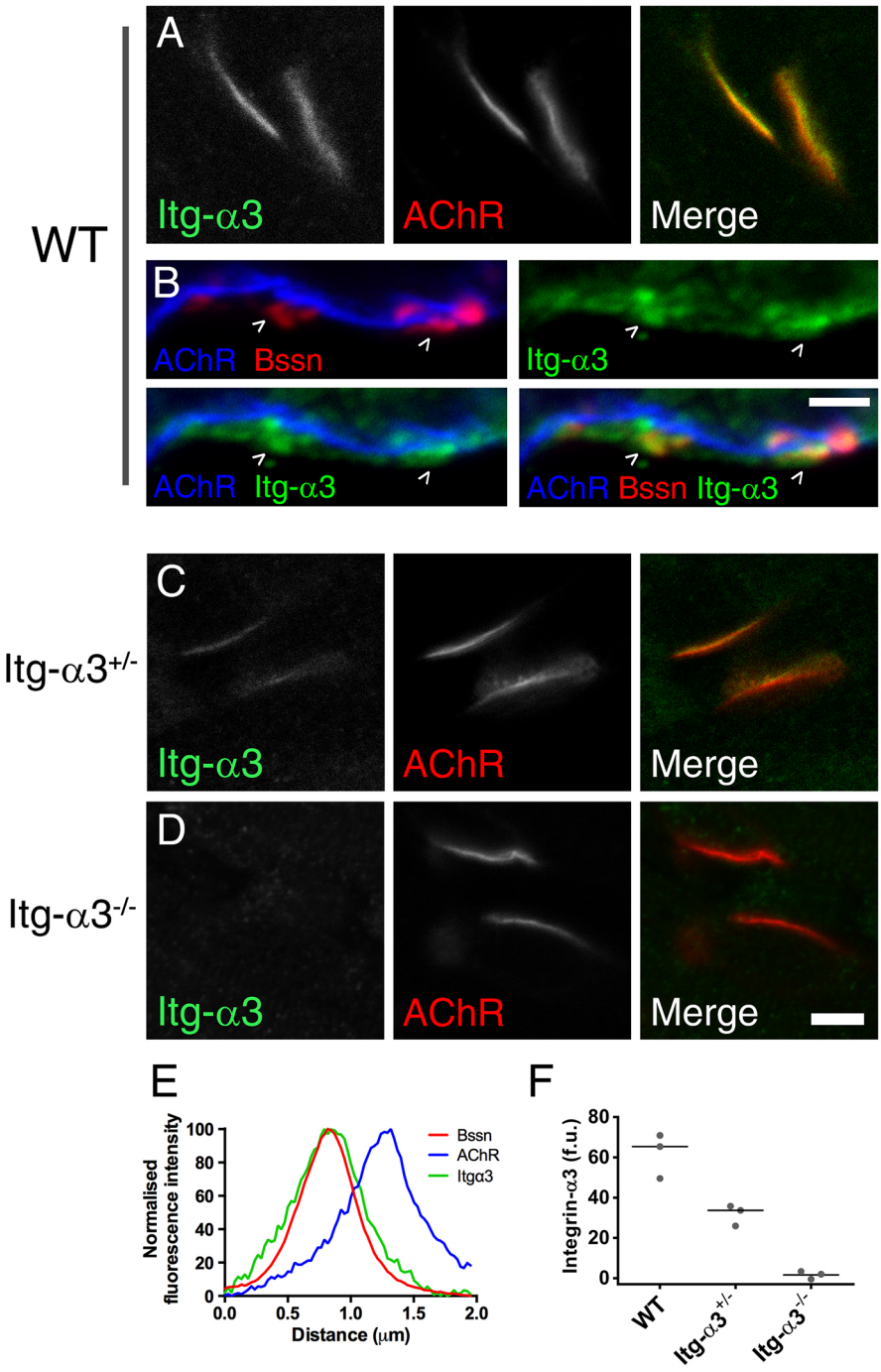

Fig. 1. Localisation of integrin-α3 at the AZs of NMJs. Immunofluorescence staining for integrin-α3 (Itg-α3) in E18.5 sternomastoid muscles from wild type (WT) (A), integrin-$\alpha3^{+/-}$ (C) and integrin-$\alpha3^{-/-}$ (D) mice. Fluorescently conjugated α-bungarotoxin was used to mark postsynaptic acetylcholine receptors (AChRs). (B) Co-labelling of integrin-α3 with presynaptic AZ marker, bassoon (Bssn), in WT E18.5 muscles. (E) Line scans across the synaptic interface, showing colocalisation of bassoon and integrin-α3, and their spatial separation with postsynaptic AChRs. (F) Fluorescence intensity of integrin-α3 staining in each genotype. Single confocal slices (A,C,D); *z*-stack of three confocal slices 0.4 µm apart, at high (×63) magnification (B). (E) Averaged traces from ten AZs across 4 WT NMJs. (F) Ten WT, 18 integrin-$\alpha3^{+/-}$ and 8 integrin-$\alpha3^{-/-}$ NMJs, taken from three animals/genotype (data points for each animal plotted with median indicated by a line). Scale bars: 5 µm (A,C,D); 2 µm (B).

Journal of Cell Science (2017) 130, 1772-1784 doi:10.1242/jcs.201103

We labelled NMJs with antibodies to three AZ markers: bassoon (encoded by *Bsn*), piccolo (encoded by *Pclo*) and P/Q VGCC (specifically the subunit encoded by *Cacna1a*). In WT mice, these proteins presented with a clear punctate staining (Nishimune et al., 2012) (Fig. 2A-C), but the fluorescence intensity of these three markers was drastically reduced in both integrin-$\alpha3^{+/-}$ and integrin-$\alpha3^{-/-}$ NMJs (Fig. 2D-I). This indicates that both complete and partial absence of integrin-α3 leads to incorrect localisation of AZ components.

Integrin-α3 directs the deposition of synaptic basal lamina at the developing NMJ

As integrins are important for the deposition and organisation of the ECM in various tissues (Conti et al., 2003; Hynes, 2002), we sought to determine whether integrin-α3 plays a role in this process at the NMJ. Using electron microscopy, we examined the ultrastructural characteristics of E18.5 NMJs. Pre- and postsynaptic elements were correctly apposed at NMJs of all three genotypes (Fig. 2J-L). In WT mice, the basal lamina, evident as a discrete electron dense layer (Chen et al., 2011; Patton et al., 2001), was clearly identifiable in the synaptic cleft (Fig. 2J; arrow). However, in integrin-$\alpha3^{+/-}$ and integrin-$\alpha3^{-/-}$ NMJs, it filled the entire span of the synaptic cleft (Fig. 2K,L), implying aberrant organisation and/or increased protein deposition. Line scans to measure pixel intensity across the cleft confirmed the paler electron-lucent portions of basal lamina adjacent to the pre- and postsynaptic membranes in WT NMJs but not in mutants (Fig. 2M). AZs were visible as small dense bodies on the presynaptic membrane,

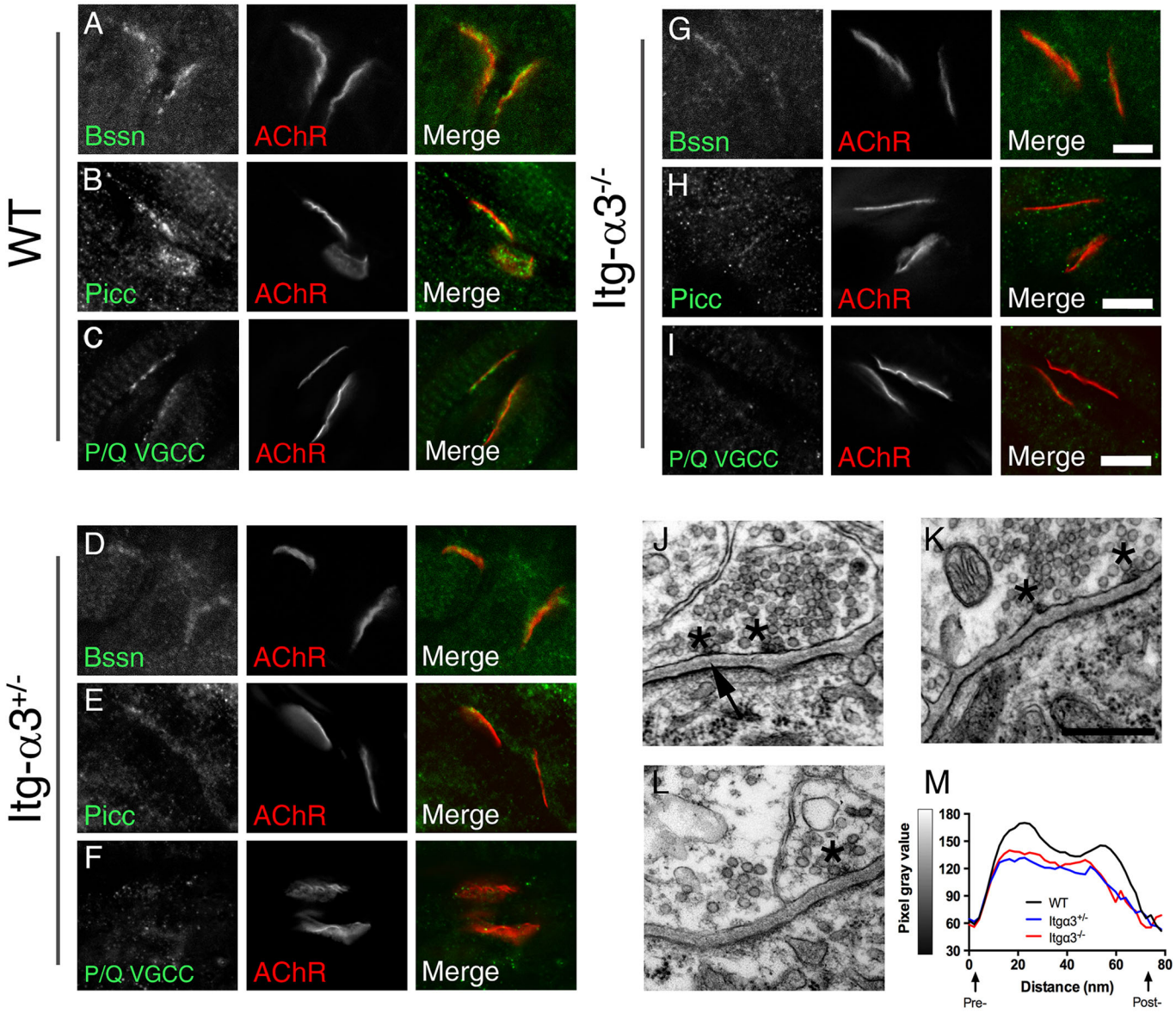

Fig. 2. Altered localisation of AZ proteins and in the organisation of basal lamina at integrin-α3-mutant NMJs during early development. Immunofluorescence staining for AZ proteins bassoon (Bssn) (A,D,G), piccolo (Picc) (B,E,H) and P/Q-type VGCCs (C,F,I) in WT (A-C), integrin-$\alpha3^{+/-}$ (D-F) and integrin-$\alpha3^{-/-}$ (G-I) sternomastoid muscles at E18.5. Electron micrographs of NMJs at ×50,000 magnification in WT (J), integrin-$\alpha3^{+/-}$ (L) and integrin-$\alpha3^{-/-}$ (K) diaphragm muscles at E18.5. Note that AZs (asterisks) were visible in all three genotypes, indicating that despite loss of some components (bassoon, piccolo and VGCCs), other core active zone proteins were present. (M) Line scans across the synaptic cleft confirmed altered basal lamina deposition: the presence of an electron-lucent space adjacent to pre- and postsynaptic membranes in WT but not mutant NMJs (also see arrow in J). Quantifications of synaptic parameters on electron micrographs are given in Table 1. Line scans are averaged from 12 NMJs/genotype, eight random measurements per NMJ. Similar results were observed across three animals/genotype. Scale bars: 5 µm (A-I), 500 nm (J-L).

Journal of Cell Science (2017) 130, 1772-1784 doi:10.1242/jcs.201103

surrounded by docked vesicles (Fig. 2J-L; asterisks). Similar numbers of AZs per µm (length) of membrane were observed in all three genotypes (Table 1), indicating that AZs were still able to form despite the partial loss of bassoon, piccolo and P/Q VGCCs (Fig. 2A-I). Similar numbers of synaptic vesicles were also observed in integrin-$\alpha3^{-/-}$ terminals compared to in WT (Table 1).

Integrin-α3 does not have an important role in muscle development

Since proper muscle development is essential for NMJ formation (Schwander et al., 2004; Yumoto et al., 2012), we investigated whether integrin-α3 is involved in myogenesis. Integrin-α3 was readily detectable by immunohistochemistry in the lungs of E18.5 WT mice (Fig. S1E). However, no signal was observed in intercostal muscle tissue throughout key phases of myogenesis (E14.5-E18.5; Fig. S1A-C) or in 8-week-old adult muscle (Fig. S1D). In addition, muscle formation appeared to proceed normally in integrin-$\alpha3^{-/-}$ mice, with peripherally nucleated muscle fibres, and deposition of laminin and collagen IV that was comparable to WT (Fig. S1G,H). At the ultrastructural level, the internal organisation of contractile filaments (myofibrils) was similar between WT and integrin-$\alpha3^{-/-}$ mice at E18.5 (Fig. S1I). These findings suggest that integrin-α3 is not present in significant quantities in muscle and has no key role in myogenesis. Therefore, given the specific localisation of integrin-α3 at the active zones (Fig. 1), it is likely that NMJ defects in mutant mice originate at the presynaptic terminus.

Involvement of integrin-α3 in AZ composition and synaptic vesicle release at adult NMJs

During the 2 weeks after birth, the NMJ undergoes several transformations. These include the growth and elaboration of the endplate from a plaque to a pretzel shape, the formation of folds in the postsynaptic membrane and the alignment of AZs with the mouths of these folds (Marques et al., 2000). While integrin-$\alpha3^{-/-}$ mice die at birth, we found that at the embryonic stages, integrin-$\alpha3^{+/-}$ mice presented with comparable defects in AZ composition (Fig. 2A-I) and synaptic basal lamina organisation (Fig. 2J-M), suggesting that mutant mice are haploinsufficient for integrin-α3 at the NMJ. We therefore used integrin-$\alpha3^{+/-}$ mice, which are viable, to investigate postnatal development of the NMJ in 2-month-old mice. In integrin-$\alpha3^{+/-}$ NMJs, immunolabelling of bassoon and piccolo was reduced compared to that in WT (Fig. 3A,B,D,E). Average fluorescence intensity of bassoon at integrin-$\alpha3^{+/-}$ NMJs was 51% of WT values (Fig. 3G), and 7% for piccolo (Fig. 3H). However, in contrast to our findings at E18.5, the immunoreactivity of P/Q VGCCs was not reduced in adult integrin-$\alpha3^{+/-}$ NMJs, and instead closely resembled that of WT (Fig. 3C,F,I). Previous studies have implicated VGCCs in the initiation of AZ assembly and clustering of bassoon (Nishimune et al., 2004). Our data reveal that reduced levels of integrin-α3 also cause a defect in AZ composition. Given the fact that P/Q VGCCs are localised normally in integrin-$\alpha3^{+/-}$ mice, but that the localisation of bassoon and piccolo are still perturbed, our results demonstrate a dependence on both VGCCs and integrin-α3 for AZ integrity. The fact that P/Q VGCCs can localise correctly in integrin-$\alpha3^{+/-}$ NMJs suggests that separate pathways might exist for the recruitment of the two proteins.

Table 1. Synaptic parameters at E18.5 and 2 months of age, quantified on electron micrographs

	WT	Integrin-$\alpha3^{+/-}$	Integrin-$\alpha3^{-/-}$
E18.5			
No. of synaptic vesicles/µm^2	48.6 (±15.3)	56.7 (±3.6)	59.7 (±10.2)
No. of active zones/µm of membrane	1.12 (±0.28)	0.89 (±0.06)	0.85 (±0.17)
2 months			
No. of synaptic vesicles/µm^2	92.0 (±5.6)	99.8 (±5.9)	–
No. of docked vesicles/active zone	6.5 (±1.1)	5.8 (±1.2)	–
No. of active zones/µm of membrane	0.78 (±0.06)	0.77 (±0.14)	–
% active zones aligned with folds	87.1 (±4.2)	81.0 (±10.5)	–
No. of folds/µm of membrane	1.3 (±0.2)	1.5 (±0.05)	–

E18.5, *n*=14-32 NMJs across two or three animals per genotype; 2 months, *n*=56-62 NMJs across three animals per genotype. Values are median±range.

To assess whether changes in AZ composition were associated with alterations in neuromuscular transmission, we used *ex vivo* diaphragm preparations for electrophysiological analysis. We assessed three parameters of neurotransmission: (i) the spontaneous release of vesicles, observed in the form of miniature endplate potentials (MEPPs); (ii) release of synaptic vesicles under nerve stimulation, observed as evoked endplate potentials (EPPs); and (iii) sustained release of neurotransmitter at high frequencies of stimulation (50 Hz). Using a physiological concentration of external Ca^{2+} at 2.5 mM, no significant difference between WTs and mutants was observed in these parameters. MEPP amplitude and frequency (Fig. 4A-C), EPP amplitudes and quantal content (number of vesicles released per stimulus) (Fig. 4D-F), and EPP amplitudes over the course of repetitive stimulation at 50 Hz were comparable across genotypes (Fig. 4G,H). In addition, EPP durations were similar between the two genotypes (WT half-width, 4.57±0.17 ms; mutant 4.30±0.14 ms; mean±s.e.m.).

Next, we decreased Ca^{2+} concentration from 2.5 to 0.3 mM. Although these concentrations are not observed *in vivo*, the reduced availability of Ca^{2+} results in a decrease in the probability of synaptic vesicle release at the AZs, and represents an experimental tool to probe in more depth the parameters of vesicle release (Del Castillo and Katz, 1953; Chand et al., 2015; Rafuse et al., 2000; Ruiz et al., 2008). Under these conditions, the EPP amplitude and quantal content were significantly reduced in integrin-$\alpha3^{+/-}$ NMJs compared to in WT (Fig. 5A-C; 51.4% reduction from WT for EPP amplitude, P=0.0017; 52.2% for quantal content, P=0.0079). In WT terminals, release sometimes exceeded ∼15 quanta; these events were notably absent in mutants (Fig. 5C). This might suggest a loss of multivesicular release events at mutant AZs and may be the result of reduced probability of release at these terminals (more severe than WTs under conditions of low Ca^{2+}). Amplitudes of spontaneous events (MEPPs) were similar between the two genotypes, indicating that the efficiency of the postsynaptic apparatus was unaffected by low Ca^{2+} (Fig. 5D, P=0.24). Next, MEPP frequency and quantal content (two indicators of synaptic vesicle release probability) were assessed over a range of Ca^{2+} concentrations. The resulting dose response data yielded sigmoid curves for each parameter, as described previously (Fig. 5E,F) (Chand et al., 2015; Ruiz et al., 2008). In each, the curve for integrin-$\alpha3^{+/-}$ NMJs was shifted to the right (towards higher concentrations of Ca^{2+}) compared to those of WT. Even though these differences were small, they were statistically significant, indicating a very slight decrease in Ca^{2+} sensitivity in integrin-$\alpha3^{+/-}$ terminals (P=0.037 for quantal content, and P=0.046 for MEPP frequency). These results, particularly the more striking impairment in evoked release at 0.3 mM Ca^{2+} concentrations (Fig. 5B,C) suggest that normal amounts of integrin-α3 are required for fully efficient neurotransmission at the NMJ.

Journal of Cell Science (2017) 130, 1772-1784 doi:10.1242/jcs.201103

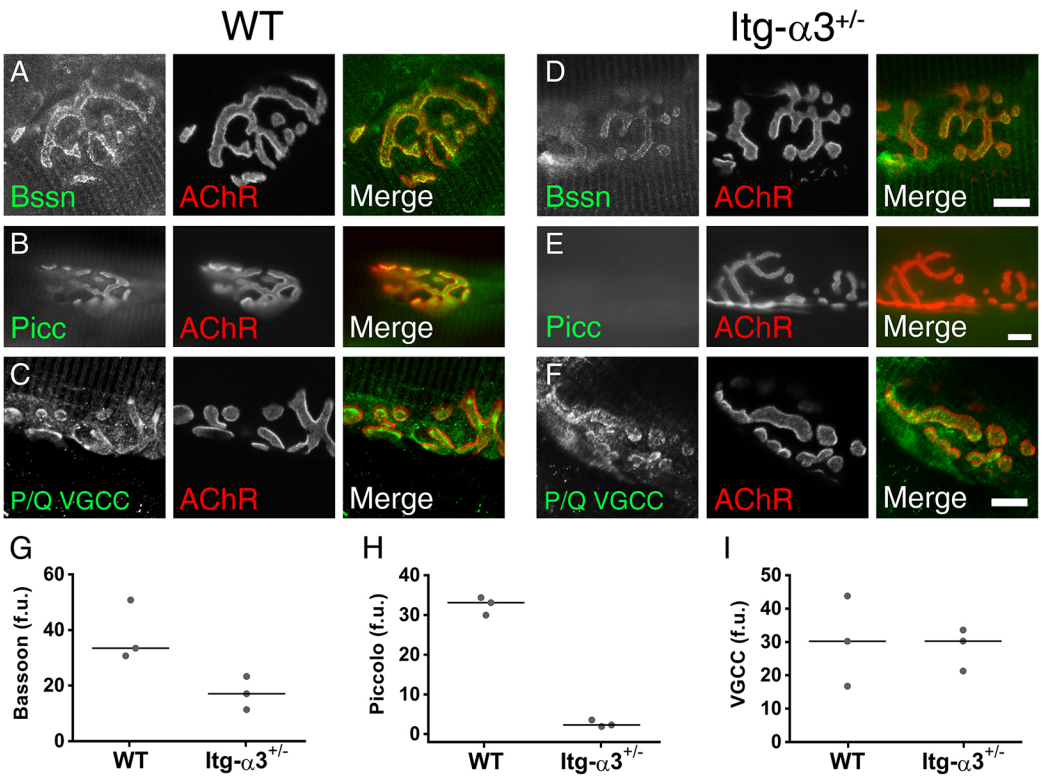

Fig. 3. Aberrant localisation of AZ proteins in NMJs of adult integrin-α3$^{+/-}$ mice. Immunofluorescence staining for AZ proteins bassoon (Bssn; A,D), piccolo (Picc; B,E) and P/Q VGCC (C,F) in WT (A-C) and integrin-α3$^{+/-}$ (D-F) sternomastoid muscles at 2 months. Fluorescence intensities were quantified in each genotype for bassoon (G), piccolo (H) and P/Q VGCC (I) from 8-13 NMJs across three animals/genotype. Data points for each animal plotted with median indicated by a line; f.u., fluorescence units. Scale bars: 10 µm.

Increased short-term facilitation and higher failure of neurotransmission at integrin-α3$^{+/-}$ NMJs

Next, we wished to determine whether integrin-α3$^{+/-}$ NMJs were associated with defects in sustained synaptic vesicle release, under conditions of reduced (0.3 mM) external Ca^{2+}. Following 50 Hz repetitive stimulation, EPPs of integrin-α3$^{+/-}$ NMJs were reduced compared to WT throughout the course of stimulation (Fig. 5G,H), in agreement with the impaired quantal release (Fig. 5A-C). Changes in short-term facilitation were evaluated next. This phenomenon occurs towards the beginning of the repetitive train, as successive stimuli yield a gradual increase in residual Ca^{2+} within terminals, and thus a corresponding escalation in response. By normalizing the EPPs to the first response in the train, differences in the initial pulse could be eliminated (Fig. 5I). Under conditions of low Ca^{2+}, NMJs of both genotypes displayed greater facilitation than at physiological conditions (compare Fig. 4G,H with Fig. 5I), reflecting the reduced baseline probability of synaptic vesicle release, and thus lower initial EPP. However, the enhanced facilitation was greater in integrin-α3$^{+/-}$ NMJs compared to those of WT. This is likely to reflect the lower response of the first stimulus in these mice, allowing the terminals to increase their output of neurotransmitter with subsequent stimuli. This phenomenon is observed in other mutants with impaired quantal release (Kong et al., 2009; Ruiz et al., 2008). Finally, no differences in the decremental response were observed between WT and integrin-α3$^{+/-}$ NMJs, again indicating that the mobilisation and reloading of vesicles was normal under reduced Ca^{2+} conditions (Fig. 5G,H).

Further examination of single stimulation events at low Ca^{2+} conditions revealed frequent failures of neurotransmission, whereby stimulation failed to elicit a recordable EPP on the postsynaptic side. Integrin-α3$^{+/-}$ NMJs suffered from significantly more failures of neurotransmission at 0.2 and 0.3 mM Ca^{2+} concentrations compared to those of WT (Fig. 5J,K; 2.4-fold over WT, P=0.0287 for 0.2 mM Ca^{2+}; 3.2-fold over WT, P=0.0328 for 0.3 mM Ca^{2+}). The increased failures in mutant mice might be expected as a direct consequence of the already reduced probability of vesicle release, and thus efficiency of neurotransmission (Fig. 5C). This has been documented in other models that display a reduced efficiency of release (Chand et al., 2015; Ruiz et al., 2008).

Altered NMJ maintenance and autophagy at integrin-α3-mutant NMJs

To determine whether integrin-α3 has a role in the postnatal maturation of plaque-shaped NMJs into topologically branched structures, we studied muscles at 2 months of age. In both WT and integrin-α3$^{+/-}$ mice, we observed pretzel-shaped endplates, with a completely overlapping presynaptic nerve terminal [labelled with antibodies to neurofilament and SV2 (encoded by *Nefm* and *Sv2a*, respectively), both in green, Fig. 6A-F]. However, the pretzel shape was often spread out over a significantly larger area in integrin-α3$^{+/-}$ NMJs, with more AChR-negative spaces within the pretzel (Fig. 6B,G; 27% increase in spread area over that of WT). However, despite the larger spread, the AChR-positive area was similar in both genotypes, indicative of a comparable extent of synaptic contact (Fig. 6H).

Various structural changes at the NMJ are known to accumulate during adulthood and ageing. To assess whether there was a difference in the way these phenotypic alterations accumulate over time, WT and integrin-α3$^{+/-}$ mice were studied at 2 and 10 months

Journal of Cell Science (2017) 130, 1772-1784 doi:10.1242/jcs.201103

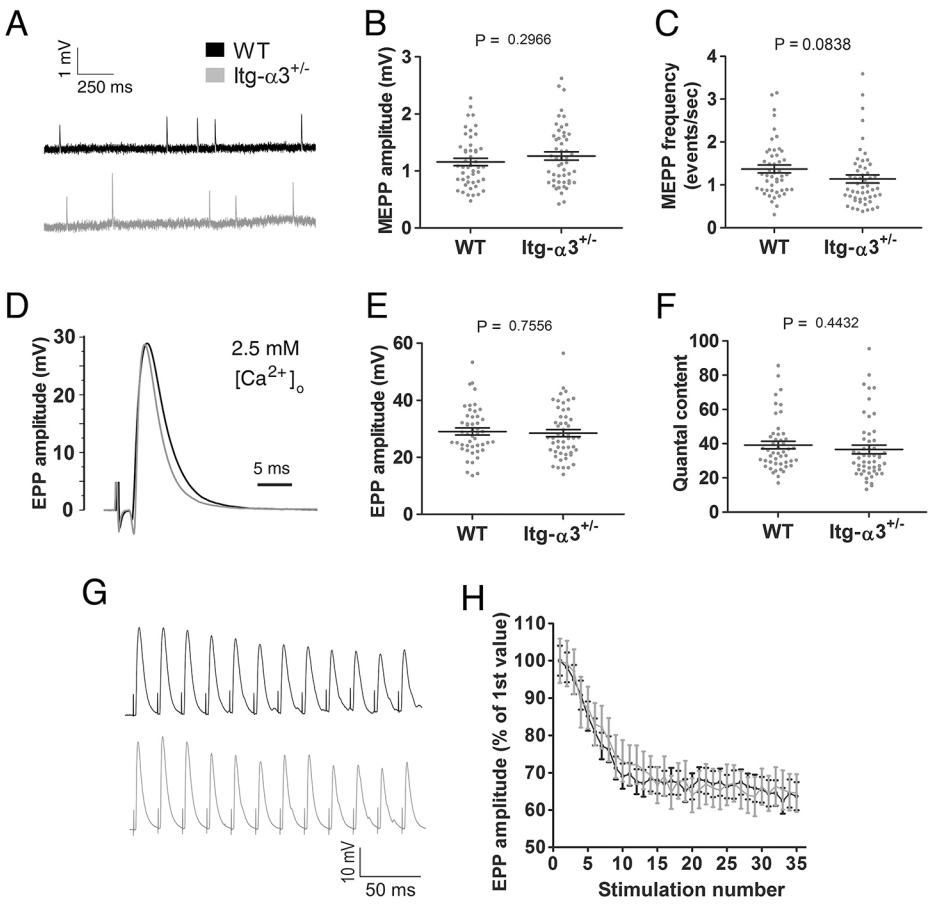

Fig. 4. Normal neurotransmission in integrin-α3$^{+/-}$ NMJs at physiological external Ca^{2+} concentrations. *Ex vivo* electrophysiology on adult (5 months) phrenic nerve and diaphragm preparations, with external buffer containing 2.5 mM Ca^{2+}. Basic parameters of neurotransmission were assessed: MEPP amplitude (A,B), MEPP frequency (A,C), EPP amplitude (D,E) and quantal content (F). No significant differences were observed in any of the parameters. Repetitive stimulation at 50 Hz (G,H). Traces were averaged and normalised to the first EPP in the train (H). Again, no differences in EPP amplitudes were observed over the course of the train. *n*=49-53 endplate recordings per genotype, across 11 animals/genotype (A-F); *n*=24-27 endplate recordings across 5-6 animals/genotype (G,H). Data are mean±s.e.m., Student's *t*-test.

of age. Certain morphological hallmarks were present at both time points, and the incidence of these was greater in integrin-α3$^{+/-}$ NMJs compared to in WT. The following observations in integrin-α3$^{+/-}$ mice are detailed below: (i) NMJs were frequently split into more fragments (Fig. 6C,I: 1.38-fold increase over that of WT at 2 months, 1.18-fold increase over that of WT at 10 months, $P<0.05$ each); (ii) NMJs presented with faint and fragmented AChR-positive clusters, always innervated by nerve inputs that were bulbous and varicose (Fig. 6D,J: 1.70-fold increase over that of WT at 2 months, $P=0.016$; not significant at 10 months, $P=0.56$); (iii) terminal nerve sprouting (Fig. 6E,K: 1.92-fold increase over that of WT at 2 months, $P=0.029$; 1.71-fold increase over that of WT at 10 months, $P=0.016$) and (iv) NMJs with excessive (three-way or more) axon branching prior to reaching the target end plate (Fig. 6F,L; 7.70-fold increase over that of WT at 2 months, $P=0.027$; 1.8-fold increase over that of WT at 10 months, $P=0.025$). These specific structural alterations have been commonly reported in aged (20-26 month old) mice (Li et al., 2011; Rudolf et al., 2014; Valdez et al., 2010) and in models of neurodegeneration (Park, 2015). Interestingly, we observed that these changes progressively accumulated in both WT and mutant mice between 2 and 10 months of age, but that the incidence of these was greater in mutants at both time points (with the exception of varicose nerve terminals, Fig. 6J).

A common feature of neurodegeneration is a dysregulation of autophagy, a key process by which the cell regulates protein quantity and quality by selective degradation in lysosomes (Cipolat Mis et al., 2016). Integrins (including α3) have been known to regulate autophagy in other systems (Chen and Debnath, 2013; Lock and Debnath, 2008), so we aimed to assess whether there were alterations in this process in integrin-α3$^{+/-}$ mice. There was a higher proportion of presynaptic terminals that stained positive for the autophagic markers p62 (encoded by *Sqstm1*) and LC3 (encoded by *Map1lc3*) in mutant compared to WT mice (Fig. 6M,O; 50% increase for p62; 37% for LC3). It is worth noting the accumulations of autophagic marker LC3 beneath the postsynaptic membranes; these often occurred irrespective of genotype and are perhaps involved in the normal turnover of AChRs and accessory proteins (Fig. 6N, arrowheads) (Carnio et al., 2014). Lysosomes were clearly visible in presynaptic terminals by electron microscopy (as vacuolated whorls of dense material) and were present in 27% of overall integrin-α3$^{+/-}$ synapses (*n*=63 NMJs across three animals) and only 14% of WT synapses (*n*=56; see Fig. 6P, arrowhead and quantification in panel O; 93% increase). Taken together, these data indicate that autophagy is upregulated in mutant mice, providing a plausible mechanism by which synaptic maintenance is altered.

Integrin-α3 is required for the connection of motoneurons to the muscle fibre

Ultrastructural elements of NMJs were examined using electron microscopy. NMJs of both genotypes appeared similar in terms of postsynaptic folding, the alignment of AZs with folds and the deposition of basal lamina (Fig. 7A,B; also see quantification in Table 1). Further analysis of electron micrographs resulted in a striking observation – portions of the nerve terminal were detached from the basal lamina in integrin-α3$^{+/-}$ NMJs but not in those of WT (Fig. 7C-D′, 13.0% overall incidence in 63 integrin-α3$^{+/-}$ synaptic boutons across three animals per genotype). In some cases, the detached terminal was partially encased with Schwann cell processes, as has been reported in the collagen XIII mouse mutant and in patients with laminin-β2 mutations, which also display a partial

Journal of Cell Science (2017) 130, 1772-1784 doi:10.1242/jcs.201103

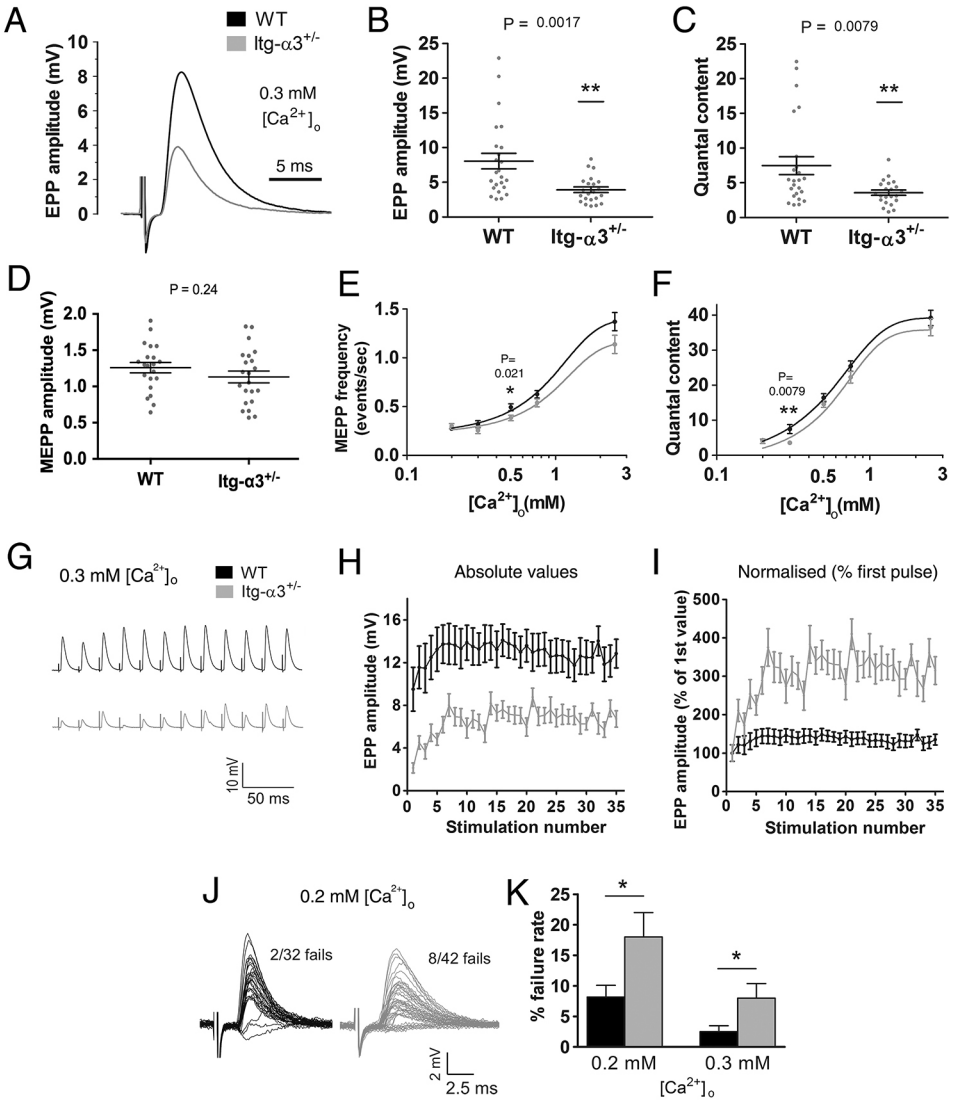

Fig. 5. Impaired synaptic vesicle release in integrin-α3$^{+/-}$ NMJs at reduced external Ca^{2+} concentrations. *Ex vivo* electrophysiology on adult (5 months) phrenic nerve and diaphragm preparations, with external buffer containing 0.3 mM Ca^{2+}. EPP amplitude (A,B) and quantal content (C) were significantly reduced in integrin-α3$^{+/-}$ NMJs compared to in WT. No difference in MEPP amplitude was observed, indicating a normal postsynaptic response (D). Two indicators of vesicle release probability, MEPP frequency (E) and quantal content (F) were plotted against varying concentrations of Ca^{2+}. Dose–response curves for integrin-α3$^{+/-}$ NMJs are significantly shifted to the right, indicating a very slightly reduced sensitivity of nerve terminals to Ca^{2+}. 50 Hz repetitive stimulation, at 0.3 mM Ca^{2+} (G-I). Traces were averaged and plotted as absolute EPP amplitude values (H), or normalised to the first EPP value in the train (I). Normalised traces revealed an enhancement in short-term facilitation over the first few stimuli in integrin-α3$^{+/-}$ NMJs over that of WT (I). Representative 1 Hz traces at 0.2 mM Ca^{2+} (J). Increased rate of neurotransmission failure in integrin-α3$^{+/-}$ endplates at 0.2 mM and 0.3 mM Ca^{2+} (K). All recordings are from 3-6 animals/genotype; *n*=22-24 recordings, except in F-H, where *n*=12-15 recordings. All graphs are mean± s.e.m., Student's *t*-test; two-way ANOVA with mixed model for panels E and F.

detachment phenotype (Latvanlehto et al., 2010; Maselli et al., 2009). Intriguingly, the basal lamina always remained localised at the postsynaptic region (Fig. 7C′,D′). One might hypothesise that nerve terminal detachment is in fact caused by Schwann cell invasion of the synaptic cleft, which in turn causes mechanical failure. However, long stretches of presynaptic membrane that lacked coverage by a Schwann cell were observed in multiple detached NMJs, making this unlikely (Fig. 7D′). The localisation of the synaptic basal lamina to the muscle suggests that the detachment is a result of mechanical failure between the nerve terminal and the basal lamina, before Schwann cell encroachment. The lack of synaptic basal lamina on the detached nerve terminals might then allow Schwann cells to intrude, since components of the synaptic basal lamina normally cause termination of Schwann cell migration.

Nerve terminals may also withdraw during neurodegeneration; however, we did not observe signs of degeneration specifically in detached NMJs (Fig. 7), and also no fully or partially denervated NMJs at under light microscopy, at either 2 or 10 months of age (Fig. 6), which suggests that terminal detachment is not secondary to neurodegeneration. These data reveal an unexpected role for integrin-α3 in mediating attachment between the presynaptic terminal and the muscle fibre.

DISCUSSION

In this study, we show that integrin-α3 regulates multiple aspects of NMJ development, function and maintenance. Consistent with its expression in nerve terminals, the localisation of AZ components and synaptic vesicle release are affected in integrin-α3-deficient mice, although gross synapse formation proceeded normally. In adulthood, integrin-α3 is also necessary for synaptic maintenance at the NMJ and for the adhesion of the nerve terminal to the muscle fibre.

Role of integrin-α3 at the AZ

Previous studies have identified integrin-α3 as an AZ component at the frog NMJ and the *Torpedo* electric synapse (which possesses structural and molecular homology to the NMJ) (Carlson et al., 2010; Cohen et al., 2000). Here, we demonstrate that integrin-α3 is also present at the AZs of mammalian NMJs (Fig. 1), where it is involved in the localisation of bassoon, piccolo and P/Q VGCCs to terminals (Fig. 2A-I; Fig. 3). Examination of NMJs using electron microscopy revealed that despite the apparent loss of these proteins in integrin-α3 mutants, AZs were still visible as small dense puncta with clustered vesicles (Fig. 2J-L). This result is analogous to the findings in mice in which the AZ protein Munc13 has been ablated; these NMJs are still able to form AZs with docked vesicles, despite Munc13 being necessary for neurotransmission (Varoqueaux et al.,

Journal of Cell Science (2017) 130, 1772-1784 doi:10.1242/jcs.201103

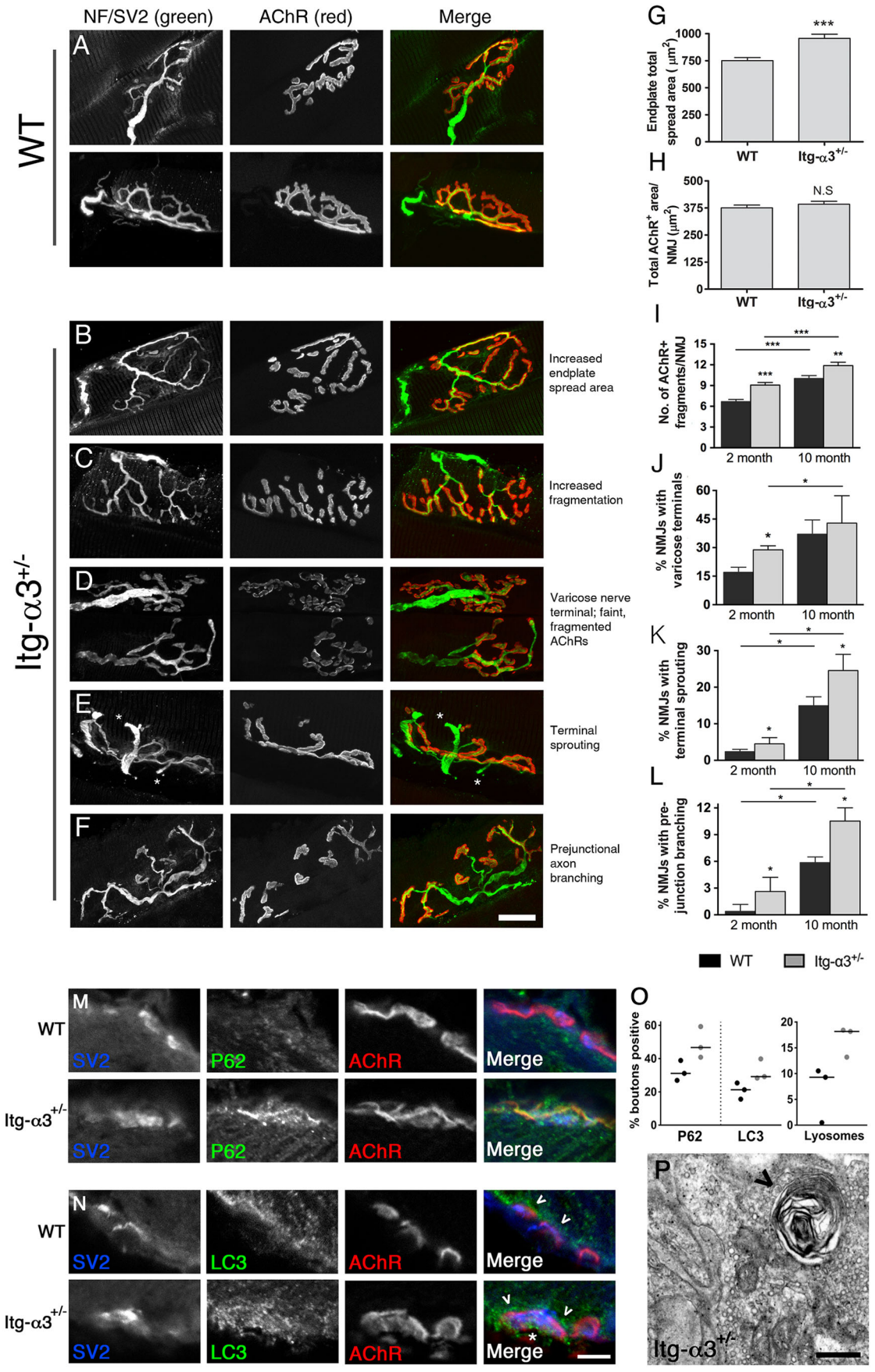

Fig. 6. See next page for legend.

Journal of Cell Science (2017) 130, 1772-1784 doi:10.1242/jcs.201103

Fig. 6. Synaptic degeneration and upregulated autophagy in NMJs of adult integrin-α3$^{+/-}$ mice. NMJs from 2-month-old WT (A) and integrin-α3$^{+/-}$ (B-F) sternomastoid muscles (nerves and AChRs labelled with anti-neurofilament and SV2 in the first column and α-bungarotoxin in the second column, respectively). The area of integrin-α3$^{+/-}$ endplates was expanded, owing to the presence of more unoccupied space within the pretzel shape (B,G), but the AChR-positive area showed no differences (H). Other NMJ characteristics indicative of ageing were analysed at ages of 2 and 10 months: increased fragmentation of endplates (C,I); NMJs with faint AChR staining, and innervation marked by bulbous varicose nerve inputs (D,J); terminal sprouting, marked by appearance of nerve sprouts exiting the innervated endplate (E,K; asterisk in E indicate terminal sprouts); excessive (three-way or more) branching of the main axon before entry into the endplate (F,L). Transverse tibialis anterior muscles from 2-month-old mice were stained with markers for autophagy: p62 (M) and LC3 (N), and the presynaptic marker SV2. Proportions of presynaptic boutons staining positive for these markers are shown in panel O. Note the frequent presence of LC3 beneath the postsynaptic membrane (arrowheads in N) as well as in presynaptic boutons (asterisk in N). By electron microscopy, the incidence of lysosomes (arrowhead in P) in presynaptic terminals was higher in mutants than WT (O,P). *n*=100-300 NMJs across 4-5 animals per genotype in panels G-L (median±interquartile range, Mann–Whitney *U*-test); 67-69 boutons across three animals/genotype in panels M-O, and 56-63 boutons across three animals per genotype for electron microscopy (O,P; data points for each animal are plotted with the median indicated by the line). Scale bars: 20 µm (A-F); 5 µm (M,N); 200 nm (P).

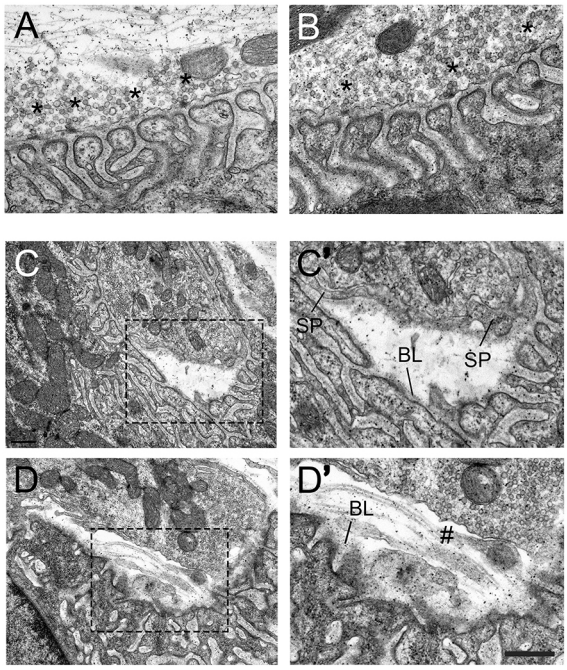

Fig. 7. Nerve terminal detachment in integrin-α3$^{+/-}$ NMJs. Electron micrographs of diaphragm NMJs from 2-month-old WT (A) and integrin-α3$^{+/-}$ (B-D′) mice. NMJs in integrin-α3$^{+/-}$ mice resembled those of WT in their ultrastructure: AZs (asterisks), postsynaptic folds and alignment of AZs with folds; full quantification of these parameters is shown in Table 1. In integrin-α3$^{+/-}$ mice, instances of nerve terminal detachment were observed (C-D′), comprising 13.0% of all boutons analysed, with none in WT. C′ and D′ are enlarged images of the regions indicated in C and D, respectively. Schwann cell processes (SP) were sometimes observed to encase parts of the detached nerve terminals. Basal lamina (BL) remains largely intact on the postsynaptic muscle side. Regions of detached nerve terminals were sometimes left exposed and without Schwann cell protrusions (marked with #). *n*=56 synaptic boutons in WT, and 63 in integrin-α3$^{+/-}$ mice, across three animals per genotype. Scale bar: 500 nm, except for C and D, where the same bar represents 1 µm.

2005). Thus, other core components of the AZ may still be able to assemble at the NMJs of Munc13 and integrin-α3 mutants.

How might integrin-α3 regulate AZ composition? The direct binding of laminin-β2 to P/Q VGCC has been shown to induce channel clustering, followed by AZ formation (Chen et al., 2011; Nishimune et al., 2004). In adult integrin-α3$^{+/-}$ mice, we observed a normal localisation of P/Q VGCC, yet the recruitment of both bassoon and piccolo was still impaired (Fig. 3). Thus, the complete configuration of the AZ may rely on multiple signals, including the laminin-β2–VGCC interaction and integrin-α3. In the *Torpedo* electric synapse, integrin-α3 co-precipitates with VGCCs, laminin-421 and spectrin (Carlson et al., 2010). Interactions with other AZ components were not confirmed in that study, but it is possible that integrin-α3 binds directly or indirectly to piccolo and bassoon to bring about their localisation at the AZ, although it is unclear why the loss of piccolo was more severe than that of bassoon. Super-resolution microscopy has shown that bassoon but not piccolo colocalises with VGCCs (Nishimune et al., 2016); this spatial separation suggests different interacting partners, and that bassoon localisation might rely on VGCCs when integrin-α3 is disrupted. Interestingly, integrins associate with actin, which has also been implicated in AZ assembly at central synapses, via interactions with bassoon, piccolo and other components (Nelson et al., 2013). Therefore, the modulation of actin dynamics might be a potential mechanism through which integrin-α3 regulates AZ composition.

Role of integrin-α3 in synaptic vesicle release at the NMJ

Ex vivo electrophysiology revealed defects in synaptic transmission at integrin-α3$^{+/-}$ NMJs, consistent with altered AZ composition. No major defects were observed under physiological (2.5 mM) concentrations of Ca^{2+} (Fig. 4). However, consistent defects in neurotransmission were revealed at low external Ca^{2+} concentrations, including impaired quantal release and increased instances of neurotransmission failure (Fig. 5). This suggests that integrin-α3 modulation of release sites might occur via interactions with the Ca^{2+} sensors that are responsible for triggering vesicle fusion, or via an effect on the opening/closing kinetics of VGCCs. *In vitro* expression studies demonstrate that bassoon positively regulates the activity of the P/Q VGCC, prolonging its opening times (Nishimune et al., 2012); therefore, the reduced localisation of bassoon at integrin-α3$^{+/-}$ NMJs might cause a decreased influx of Ca^{2+} at these terminals, which would be exacerbated when the concentration of external Ca^{2+} is reduced.

Given the deficiency of bassoon and piccolo at adult integrin-α3$^{+/-}$ AZs (Fig. 3), one might expect more significant defects in neurotransmitter release at physiological Ca^{2+} conditions. However, these results are consistent with previous findings, which demonstrated no major electrophysiological defects in hippocampal slices from piccolo-mutant mice or in cultured cortical neurons in which both bassoon and piccolo had been disrupted (Mukherjee et al., 2010). By contrast, bassoon is important for maintaining sustained neurotransmitter release during short trains at central synapses of the visual and auditory systems. These rely on frequencies of repetitive release that are much higher than those that occur at the NMJ, although defects are also apparent at low (20 Hz) frequency stimulation (Hallermann et al., 2010; Schulz et al., 2014). One possibility is that defects in integrin-α3$^{+/-}$ NMJs could become apparent after longer durations or higher frequencies of sustained neurotransmitter release. All in all, the roles of bassoon and/or piccolo appear to vary across different synapses.

Role of integrin-α3 in NMJ maintenance

We have also found that integrin-α3 is important for the maintenance of synaptic integrity at the NMJ. Adult integrin-α3$^{+/-}$ mice display NMJs with characteristics that are frequently observed in aged

(~2 year old) mice (Li et al., 2011; Rudolf et al., 2014), and in models of neurodegeneration such as amyotrophic lateral sclerosis (ALS) (Park, 2015), even at 2 months of age (Fig. 6). Similar defects are also observed in mutants for laminin-α4, collagen IV (the α5 chain), collagen XIII and nidogen-2, suggesting that interactions between a range of basal lamina proteins and integrins may be important for synaptic maintenance (Fox et al., 2007, 2008; Latvanlehto et al., 2010; Samuel et al., 2012). Consistent with this finding is altered autophagy (Fig. 6M-P), a common factor in the causation and/or progression of pathology in models of neurodegeneration, including at the NMJ (Carnio et al., 2014; Cipolat Mis et al., 2016). As a mechanism of protein degradation, increased autophagy is thought to be a cause of synaptic breakdown in motoneuron diseases; it might also represent a protective mechanism to remove faulty proteins and organelles resulting from neurodegenerative pathology (Cipolat Mis et al., 2016).

Unexpectedly, ultrastructural analysis revealed instances of detachment of the nerve terminal from the basal lamina in integrin-α3-mutant NMJs (Fig. 7). Previous studies have shown that defects in a number of ECM proteins are associated with reduced nerve adhesion at the NMJ. These proteins include collagen XIII in the mouse, laminin-β2 in humans (who present with congenital myasthenia), and collagen IV and laminin A in *Drosophila* (Koper et al., 2012; Latvanlehto et al., 2010; Maselli et al., 2009). However, despite comprehensive interrogation by genetic means, no cell surface receptors have been identified (Koper et al., 2012). To our knowledge, our data are the first report of a receptor mediating anchorage of the nerve terminal to the muscle. It has been hypothesised that multiple receptors are likely to mediate this attachment, but our results show that even hemizygous ablation of integrin-α3 is enough to cause detachment. As this defect was not detected in mutant embryos, it suggests that the detachment of nerve terminals in 2-month-old mice occurs following mechanical stresses incurred during postnatal muscle activity. The resulting widening of the cleft might result in reduced MEPP and EPP sizes in affected NMJs owing to dilution of neurotransmitter in the intervening space. Additional studies will be required to address these points.

Previous studies on integrins at the NMJ

Previous roles for integrin subunits have been identified in several model organisms. In the mouse, conditional knockout of integrin-β1 in muscle results in defects in AChR clustering and a failure of motoneurons to terminate at the muscle midline. In contrast, specific ablation of integrin-β1 in motoneurons (disrupting the formation of all integrin-β1-containing heterodimers, including α3β1) causes no gross abnormalities at the NMJ, although the investigators did not analyse AZs, synaptic transmission or ultrastructure (Schwander et al., 2004). Our findings are consistent at this level, whereby general development and patterning of the NMJs of integrin-α3 mutants appear normal.

In *Drosophila*, ablation of integrin-αPS1, the orthologue with the closest identity to mammalian integrin-α3, also resulted in no obvious morphological or structural change at the NMJ (Narasimha and Brown, 2013; Prokop et al., 1998). Roles for the two *Drosophila* integrin-β subunits in the regulation of NMJ size have been subsequently found (Beumer et al., 1999; Tsai et al., 2012). NMJs of integrin-αPS3 knockouts grow to a larger size, and neurotransmitter release show a gain of function, with abnormally large evoked currents and an increased frequency of spontaneous release compared to those of WT (Rohrbough et al., 2000). However, it should be noted that the repertoire of integrins is much smaller in *Drosophila* than in mammals (five α- and two β-subunits versus 18 α- and 8 β-subunits in mammals), and several of the subunits, including integrin-αPS3 have no clear orthology with particular mammalian isoform(s) (Narasimha and Brown, 2013). In addition, the NMJs of *Drosophila* are evolutionarily distinct from those of vertebrates, in that they are glutamatergic rather than cholinergic, and possess a different molecular arrangement at the AZ (Maglione and Sigrist, 2013). Therefore, caution should probably be exercised when comparing the roles of integrin isoforms between species.

Other functions for integrins at the NMJ have been identified in frogs. Eccentric muscle stretch and mild hypertonicity result in increased synaptic vesicle release at the frog NMJ, an effect which is mediated by integrins (Chen and Grinnell, 1997; Kashani et al., 2001). However, mechanical stretch effects are noticeably absent at the mouse NMJ (Grinnell et al., 2004; Hutter and Trautwein, 1956), although it would be interesting to determine whether the effects of hypertonicity are also mediated by integrins in mammals. The studies in frog muscle utilised RGD peptides to pharmacologically disrupt several possible integrins, but this would have excluded integrin-α3 (Hynes, 2002); however, one cannot rule out overlapping involvements of multiple isoforms.

Conclusions

These results reveal multiple roles for integrin-α3 at the NMJ – in the localisation of AZ components and neurotransmission, and also in structural maintenance at the NMJ. Despite these findings, adult integrin-α3$^{+/-}$ mice have no overt phenotype. Electrophysiological defects were apparent under conditions of low rather than physiological Ca^{2+} concentrations, and as such might not result in strength deficits. Instead, we hypothesise that progressive defects in synaptic maintenance might impact on integrin-α3$^{+/-}$ mice in later stages of life than those analysed here. Patients with homozygous mutations in the *ITGA3* gene have recently been identified, although they do not survive beyond early infancy, also due to defects in multiple organ systems, analogous to what is reported for integrin-α3$^{-/-}$ mice (Has et al., 2012). The patients however presented with muscular hypotonia, which is suggestive of neuromuscular defects, although analysis of synaptic transmission was not performed. A mouse model with motoneuron-specific ablation of both alleles of *Itga3* might allow for further elucidation of the functions of this protein at the NMJ as well as of the effects of knocking out both alleles in adults. Although we saw no immunolabelling of integrin-α3 in the muscle tissue (Fig. S1), a conditional knockout would conclusively exclude effects of possible dysfunction in other tissues (which might include the central nervous system, blood vessels and skin). While early lethality follows complete loss of integrin-α3, our results show that alterations in protein function (perhaps caused by loss of expression or missense mutations), although compatible with life, could lead to NMJ dysfunction. This work also has implications for our overall understanding of synaptic function and opens up new avenues to explore the functions of adhesion receptors at the NMJ.

MATERIALS AND METHODS

Integrin-α3-knockout mice

Mutant mice (background strain C57BL6/129) were housed and bred at Barts Cancer Institute, Queen Mary University of London, in accordance with the Animals (Scientific Procedures) Act 1986. Animals were killed by cervical dislocation in accordance with Schedule 1 of the Act. Embryos at E18.5 were collected from mothers and decapitated immediately before dissection. For analysis of adult tissue, animals were cardiac-perfused under anaesthesia with 4% PFA, pH 7.4 (immunohistochemical stains) or 2% PFA with 1.5% glutaraldehyde in 0.1 M cacodylate buffer, pH 7.4 (electron microscopy).

Antibodies

Primary antibodies were as follows: rabbit anti-integrin-α3, 1:100 (Kreidberg et al., 1996); mouse anti-bassoon, 1:500 (cat. no. GTX13249,

SAP7F407, Source BioScience, Nottingham, UK); rabbit anti-piccolo, cat. no. 142002, 1:200, and rabbit anti-P/Q-VGCC ($Ca_v2.1$), cat. no. 152203, 1:300 (Synaptic Systems, Göttingen, Germany); mouse anti-synaptic vesicle protein 2 (SV2), cat. no. SV2, 1:100 (Developmental Studies Hybridoma Bank, Iowa City, IA); mouse anti-neurofilament 160 kDa, cat. no. N5264, 1:200 (NN18, Sigma); rabbit anti-LC3, cat. no. APG8A, 1:200 (Abgent, San Diego, CA) and rabbit anti-p62, cat. no. P0067, 1:200 (Sigma). Alexa-Fluor-594-conjugated α-bungarotoxin (1:1000, Invitrogen, cat. no. B13423) was added simultaneously with secondary antibodies (1:500, Invitrogen, varieties of Alexa Fluor-488-conjugated, -594-conjugated and -647-conjugated anti-mouse and anti-rabbit IgG antibodies (A-11034, A-11001, A-11005, R37117, A-21235, A-21245) to mark AChRs (Invitrogen, Paisley, UK).

Immunohistochemistry for AZ and NMJ morphology analysis

4% PFA in PBS was used to fix dissected muscles from E18.5 embryos for 2 h, or for cardiac perfusion of 2-month-old mice. After four washes in PBS over 2 h, sternomastoid muscles were cryoprotected in PBS with 30% sucrose for 2 h, blotted on paper towel, embedded in OCT medium (RA Lamb, Eastbourne, UK) and frozen in liquid-nitrogen-cooled isopentane. 25 µm longitudinal sections were cut to capture whole NMJs. Four subsequent wash steps were performed in PBS over a total of 1 h. After rehydration in PBS, samples were permeabilised in PBS with 0.1% Triton for 40 min, washed and incubated with PBS containing 1:40 Mouse on Mouse block (Vector Laboratories, Peterborough, UK) for 2.5 h. Samples were blocked in PBS with 10% goat serum (Sigma) for 1.5 h, followed by incubation with primary antibodies overnight in blocking buffer. Samples were washed, incubated with secondary antibodies for 3 h and washed again. Samples were mounted in Prolong Gold Antifade (Invitrogen).

Ex vivo electrophysiology

Experimental procedures on 5-month-old mice were performed as described previously (Webster et al., 2013). Phrenic nerve and hemidiaphragm preparations were bathed in Krebs–Henseleit buffer under 95% O_2 with 5% CO_2 (NaCl 118 mM, KCl 4.7 mM, $MgSO_4.7H_2O$ 1.2 mM, H_2KO_4P 1.2 mM, $NaHCO_3$ 24.9 mM, glucose 10 mM, $CaCl_2$ 2.5 mM). For experiments with reduced external concentration of Ca^{2+} $[CaCl_2]_o$ (concentrations 0.2 mM, 0.3 mM, 0.5 mM, 0.75 mM in Krebs–Henseleit buffer), preparations were rinsed and bathed in the relevant solution for 10 min before recording. The preparation was rinsed and bathed in lower $[CaCl_2]_o$ solution for 10 min before recordings. Experiments took place in a Faraday enclosure at room temperature (20-22°C). Phrenic nerve was stimulated with a solid-state square wave pulse generator (Grass Instruments, Quincy, MA) via a suction electrode. The signal was amplified using an Axoclamp-2A amplifier (Molecular Devices, Sunnyvale, CA). Blockade of muscle contraction was achieved with 2.5 µM µ-conotoxin GIIIB (Alomone Labs, Jerusalem, Israel). A 25 min incubation (and subsequent rinse) blocked contraction for the 1.5 h recording period. A borosilicate glass electrode (10-15 MΩ resistance, filled with 3 M KCl) was used for recording MEPPs and EPPs from individual muscle fibres. A micromanipulation rig (Scientifica, Maidenhead, UK) was used to place electrodes as near to the endplate region as possible (MEPP rise time <1.5 ms), with visualisation under a BX51WI stereomicroscope (Olympus, Southend-on-Sea, UK). Recordings were analysed using pCLAMP 9 software (Molecular Devices) and normalised to a −80 mV baseline, thus correcting for differences in resting membrane potential. For determination of quantal content, EPP amplitude was subjected the further species specific correction, as follows:

$$AMP_{EPP} = AMP_{EPP(measured)}/[1 - 0.8\ AMP_{EPP(measured)}/E],$$

where AMP_{EPP} is the EPP amplitude, 0.8 the correction factor for mouse endplates (McLachlan and Martin, 1981) and E is the resting membrane potential (−80 mV). Quantal content was calculated according to the following formula:

$$\text{Quantal content} = \text{mean}(AMP_{EPP})/\text{mean}(AMP_{MEPP}),$$

where AMP_{MEPP} is the MEPP amplitude.

Electron microscopy

Fixation of thoraxes from E18.5 mice immediately after death or to cardiac perfusion of 2-month-old adults were performed using 2% PFA and 1.5% glutaraldehyde in 0.1 M cacodylate buffer, pH 7.4. Diaphragms were dissected for further processing. The following steps were performed: post fixation in 1% OsO_4 with 0.1 M cacodylate buffer, pH 7.3 at 3°C for 12 h; washes in 0.1 M cacodylate buffer, pH 7.4; enbloc staining in 0.5% uranyl acetate in dH_2O at 3°C for 30 min. After rinsing in dH_2O, specimens were dehydrated in a graded ethanol–water series and infiltrated with Agar 100 resin before hardening. 70-nm ultrathin sections were cut and collected on 300-mesh copper grids, and stained with lead citrate. Sections were viewed and images of NMJs were recorded at ×20,000-50,000 magnification, using a Jeol 1010 transmission electron microscope.

Genotyping of integrin-α3-knockout mice by performing PCR

DNA extraction and PCR amplification of the integrin-α3 gene was performed as described previously (DiPersio et al., 1997; Truett et al., 2000). Primers were as follows – WT (from integrin-α3 gene) 5′-CCGTC-TATGTCTTCATGAACC-3′; integrin-α3 knockout (from neomycin resistance gene) 5′-GGGGAACTTCCTGACTAG-3′; common (from integrin-α3 gene) 5′-GGAATCCATCCTGGTTGATGTC (Invitrogen). After denaturation at 94°C for 2 min, 30 cycles were performed: 30 s at 94°C (denaturation), 40 s at 55°C (extension) and 30 s at 72°C (annealing).

Imaging, quantification and statistics

For reconstruction of whole *en face* NMJs in the adult, 0.4 µm slices were taken using a Zeiss LSM 710 confocal microscope and projected as a *z*-stack using the maximal pixel intensity in ImageJ, as described previously (Chen et al., 2011). For imaging of bassoon and integrin-α3 staining in NMJs at E18.5, individual confocal slices were used. For imaging of piccolo and P/Q VGCCs at E18.5, single slices were resolved using three-dimensional (3D) deconvolution, to improve the signal-to-background ratio. A *z*-series was acquired at 0.4 µm intervals using a Leica DM4000 wide-field microscope, which is the optimal distance as determined using the Nyquist calculation (http://www.svi.nl/NyquistCalculator) and known acquisition parameters (oil immersion ×63 objective, refractive index of mounting medium 1.515; numerical aperture, 1.25). A point-spread function was derived experimentally using 1µm fluorescent Fluosphere beads (Invitrogen) and the same acquisition parameters. 3D deconvolution was performed with Autoquant X3 software (Autoquant Imaging Inc, Rockville, MD). All images were initially assembled using ImageJ, and whole figures were constructed in Adobe Photoshop. Image processing (linear brightness and contrast) was applied to all image panels to the same extent.

For measurements of adult NMJ morphology in ImageJ, only junctions in an *en face* orientation were assessed. Total area and expansion of the pretzel shape was measured by tracing the circumference of each NMJ, encompassing any negative space. The area of the AChR-positive region alone was measured by thresholding the image by pixel intensity, to exclude negative spaces. Fragmentation was measured as the number of discrete AChR clusters per NMJ. In electron microscopy sections, the alignment of AZs was defined as follows. A line was drawn as the trajectory from the walls of the folds to the nerve terminal. If this line crossed an AZ, it was considered aligned.

Line scans to assess colocalisation of bassoon, integrin-α3 and AChRs in WT E18.5 NMJs were taken in ImageJ. Pixel intensities for each channel were normalised to the lowest pixel intensity within each line scan, to account for background. Only raw pixel intensity information was used for line scans in electron microscopy sections. For comparison of fluorescence intensities for integrin-α3, bassoon, piccolo and P/Q VGCC, a small selection of 15×15 pixel areas were used to sample and average the pixel intensities at ten random points per NMJ, and the resulting average was normalised to the background signal surrounding the NMJ. Each staining was performed in isolation to avoid possible quenching by other dyes.

For electron microscopy and immunohistochemical experiments, multiple NMJs were averaged to give a single value for each animal; these values were then plotted as single data points (as advised in Vaux, 2012). Where n=3 animals, these points were plotted to show the median and each of the 3 values, and statistical tests were not performed. Where n>4-5 animals, values

were plotted as bars with median±interquartile range (IQR), and a Mann–Whitney *U*-test was performed to assign statistical significance. For electrophysiological experiments, each point plotted represents averaged recordings from a single NMJ, with multiple NMJs from several animals (details in the figure legends). Statistical analyses were performed in two ways: (1) taking each NMJ as an individual '*n*' number (Student's *t*-test, two-tailed) and (2) taking each animal as an individual '*n*' (Mann–Whitney *U*-test). A two-way ANOVA was used to analyse dose–response curves of quantal content and MEPP frequency at varying $[CaCl_2]_o$ values (concentration of $CaCl_2$ in external buffer), using $[CaCl_2]_o$ and a categorical variable for the mouse model (WT, integrin-$\alpha3^{+/-}$) as independent variables. A mixed model was further applied to account for the fact that the variance was higher between different mice than within an individual mouse. Significance thresholds were set as $P<0.05$ (*), $P<0.01$ (**) and $P<0.001$ (***); N.S., not significant.

Acknowledgements
The authors thank Bertrand Vernay for assistance with deconvolution microscopy, and Jennifer Morgan for critical feedback on the work. Also Bruce Williams and Julie Holdsworth for their technical assistance with animal maintenance and procedures.

Competing interests
The authors declare no competing or financial interests.

Author contributions
Conceptualisation: J.A.R., Y.J., K.H.-D., F.J.C., R.G.W. Validation: J.A.R., R.G.W. Formal analysis: J.A.R., R.G.W., H.C., F.J.C.; Investigation: J.A.R., R.G.W., T.L., L. E.R., M.T., M.B., F.J.C.; Resources: F.M., D.B., K.H.-D., F.J.C.; Writing - original draft: J.A.R., F.J.C.; Writing - review & editing: J.A.R., R.G.W., T.L., L.E.R., M.T., M.B., Y.J., H.C., F.M., D.B., K.H.-D., F.J.C.; Visualisation: J.A.R., F.J.C.; Supervision: F.J.C.; Project administration: F.J.C.; Funding acquisition: F.J.C.

Funding
This work was supported by the Biomedical Research Centre, Association Francaise Contre les Myopathies (AFM-Téléthon; grant 14572); Great Ormond Street Hospital Charity and University College London Impact to J.A.R.; Cancer Research UK to T.L., L.E.R. and K.H.-D.; Austrian Science Fund (FWF) to H.C.; and Medical Research Council grant MR/M006824 to R.G.W. and D.B. Deposited in PMC for release after 6 months.

Supplementary information
Supplementary information available online at
http://jcs.biologists.org/lookup/doi/10.1242/jcs.201103.supplemental

References
Beumer, K. J., Rohrbough, J., Prokop, A. and Broadie, K. (1999). A role for PS integrins in morphological growth and synaptic function at the postembryonic neuromuscular junction of Drosophila. *Development* **126**, 5833-5846.
Carlson, S. S., Valdez, G. and Sanes, J. R. (2010). Presynaptic calcium channels and α3-integrins are complexed with synaptic cleft laminins, cytoskeletal elements and active zone components. *J. Neurochem.* **115**, 654-666.
Carnio, S., LoVerso, F., Baraibar, M. A., Longa, E., Khan, M. M., Maffei, M., Reischl, M., Canepari, M., Loefler, S., Kern, H. et al. (2014). Autophagy impairment in muscle induces neuromuscular junction degeneration and precocious aging. *Cell Rep.* **8**, 1509-1521.
Chand, K. K., Lee, K. M., Schenning, M. P., Lavidis, N. A. and Noakes, P. G. (2015). Loss of β2-laminin alters calcium sensitivity and voltage-gated calcium channel maturation of neurotransmission at the neuromuscular junction. *J. Physiol.* **593**, 245-265.
Chen, N. and Debnath, J. (2013). IκB kinase complex (IKK) triggers detachment-induced autophagy in mammary epithelial cells independently of the PI3K-AKT-MTORC1 pathway. *Autophagy* **9**, 1214-1227.
Chen, B. M. and Grinnell, A. D. (1997). Kinetics, Ca^{2+} dependence, and biophysical properties of integrin-mediated mechanical modulation of transmitter release from frog motor nerve terminals. *J. Neurosci.* **17**, 904-916.
Chen, J., Billings, S. E. and Nishimune, H. (2011). Calcium channels link the muscle-derived synapse organizer laminin β2 to Bassoon and CAST/Erc2 to organize presynaptic active zones. *J. Neurosci.* **31**, 512-525.
Cipolat Mis, M. S., Brajkovic, S., Frattini, E., Di Fonzo, A. and Corti, S. (2016). Autophagy in motor neuron disease: key pathogenetic mechanisms and therapeutic targets. *Mol. Cell. Neurosci.* **72**, 84-90.
Cohen, M. W., Hoffstrom, B. G. and DeSimone, D. W. (2000). Active zones on motor nerve terminals contain alpha3beta1 integrin. *J. Neurosci.* **20**, 4912-4921.
Conti, F. J. A., Rudling, R. J., Robson, A. and Hodivala-Dilke, K. M. (2003). Alpha3beta1 integrin regulates hair follicle but not interfollicular morphogenesis in adult epidermis. *J. Cell Sci.* **116**, 2737-2747.
Del Castillo, J. and Katz, B. (1953). Statistical nature of "facilitation" at a single nerve–muscle junction. *Nature* **171**, 1016-1017.
DiPersio, C. M., Hodivala-Dilke, K. M., Jaenisch, R., Kreidberg, J. A. and Hynes, R. O. (1997). Alpha3beta1 integrin is required for normal development of the epidermal basement membrane. *J. Cell Biol.* **137**, 729-742.
Fox, M. A., Sanes, J. R., Borza, D.-B., Eswarakumar, V. P., Fässler, R., Hudson, B. G., John, S. W. M., Ninomiya, Y., Pedchenko, V., Pfaff, S. L. et al. (2007). Distinct target-derived signals organize formation, maturation, and maintenance of motor nerve terminals. *Cell* **129**, 179-193.
Fox, M. A., Ho, M. S. P., Smyth, N. and Sanes, J. R. (2008). A synaptic nidogen: developmental regulation and role of nidogen-2 at the neuromuscular junction. *Neural Dev.* **3**, 24.
Grinnell, A. D., Chen, B.-M., Kashani, A., Lin, J., Suzuki, K. and Kidokoro, Y. (2004). The role of integrins in the modulation of neurotransmitter release from motor nerve terminals by stretch and hypertonicity. *J. Neurocytol.* **32**, 489-503.
Hallermann, S., Fejtova, A., Schmidt, H., Weyhersmüller, A., Silver, R. A., Gundelfinger, E. D. and Eilers, J. (2010). Bassoon speeds vesicle reloading at a central excitatory synapse. *Neuron* **68**, 710-723.
Has, C., Spartà, G., Kiritsi, D., Weibel, L., Moeller, A., Vega-Warner, V., Waters, A., He, Y., Anikster, Y., Esser, P. et al. (2012). Integrin α3 mutations with kidney, lung, and skin disease. *N. Engl. J. Med.* **366**, 1508-1514.
Hutter, O. F. and Trautwein, W. (1956). Neuromuscular facilitation by stretch of motor nerve-endings. *J. Physiol.* **133**, 610-625.
Hynes, R. O. (2002). Integrins: bidirectional, allosteric signaling machines. *Cell* **110**, 673-687.
Kashani, A. H., Chen, B.-M. and Grinnell, A. D. (2001). Hypertonic enhancement of transmitter release from frog motor nerve terminals: Ca^{2+} independence and role of integrins. *J. Physiol.* **530**, 243-252.
Kong, L., Wang, X., Choe, D. W., Polley, M., Burnett, B. G., Bosch-Marcé, M., Griffin, J. W., Rich, M. M. and Sumner, C. J. (2009). Impaired synaptic vesicle release and immaturity of neuromuscular junctions in spinal muscular atrophy mice. *J. Neurosci.* **29**, 842-851.
Koper, A., Schenck, A. and Prokop, A. (2012). Analysis of adhesion molecules and basement membrane contributions to synaptic adhesion at the Drosophila embryonic NMJ. *PLoS ONE* **7**, e36339.
Kreidberg, J. A., Donovan, M. J., Goldstein, S. L., Rennke, H., Shepherd, K., Jones, R. C. and Jaenisch, R. (1996). Alpha3beta1 integrin has a crucial role in kidney and lung organogenesis. *Development* **122**, 3537-3547.
Latvanlehto, A., Fox, M. A., Sormunen, R., Tu, H., Oikarainen, T., Koski, A., Naumenko, N., Shakirzyanova, A., Kallio, M., Ilves, M. et al. (2010). Muscle-derived collagen XIII regulates maturation of the skeletal neuromuscular junction. *J. Neurosci.* **30**, 12230-12241.
Li, Y., Lee, Y. and Thompson, W. J. (2011). Changes in aging mouse neuromuscular junctions are explained by degeneration and regeneration of muscle fiber segments at the synapse. *J. Neurosci.* **31**, 14910-14919.
Lock, R. and Debnath, J. (2008). Extracellular matrix regulation of autophagy. *Curr. Opin. Cell Biol.* **20**, 583-588.
Maglione, M. and Sigrist, S. J. (2013). Seeing the forest tree by tree: super-resolution light microscopy meets the neurosciences. *Nat. Neurosci.* **16**, 790-797.
Marques, M. J., Conchello, J. A. and Lichtman, J. W. (2000). From plaque to pretzel: fold formation and acetylcholine receptor loss at the developing neuromuscular junction. *J. Neurosci.* **20**, 3663-3675.
Maselli, R. A., Ng, J. J., Anderson, J. A., Cagney, O., Arredondo, J., Williams, C., Wessel, H. B., Abdel-Hamid, H. and Wollmann, R. L. (2009). Mutations in LAMB2 causing a severe form of synaptic congenital myasthenic syndrome. *J. Med. Genet.* **46**, 203-208.
McLachlan, E. M. and Martin, A. R. (1981). Non-linear summation of end-plate potentials in the frog and mouse. *J. Physiol.* **311**, 307-324.
Meriney, S. D. and Dittrich, M. (2013). Organization and function of transmitter release sites at the neuromuscular junction. *J. Physiol.* **591**, 3159-3165.
Mukherjee, K., Yang, X., Gerber, S. H., Kwon, H.-B., Ho, A., Castillo, P. E., Liu, X. and Südhof, T. C. (2010). Piccolo and bassoon maintain synaptic vesicle clustering without directly participating in vesicle exocytosis. *Proc. Natl. Acad. Sci. USA* **107**, 6504-6509.
Narasimha, M. and Brown, N. H. (2013). Integrins and Associated Proteins in Drosophila Development. In *Integrins and development* (Ed. E. Danen). Madame Curie Bioscience Database [Internet]. Austin, TX, Landes Bioscience.
Nelson, J. C., Stavoe, A. K. H. and Colón-Ramos, D. A. (2013). The actin cytoskeleton in presynaptic assembly. *Cell Adh. Migr.* **7**, 379-387.
Nishimune, H., Sanes, J. R. and Carlson, S. S. (2004). A synaptic laminin-calcium channel interaction organizes active zones in motor nerve terminals. *Nature* **432**, 580-587.
Nishimune, H., Numata, T., Chen, J., Aoki, Y., Wang, Y., Starr, M. P., Mori, Y. and Stanford, J. A. (2012). Active zone protein Bassoon co-localizes with presynaptic calcium channel, modifies channel function, and recovers from aging related loss by exercise. *PLoS ONE* **7**, e38029.

Nishimune, H., Badawi, Y., Mori, S. and Shigemoto, K. (2016). Dual-color STED microscopy reveals a sandwich structure of Bassoon and Piccolo in active zones of adult and aged mice. *Sci. Rep.* **6**, 27935.
Park, K. H. J. (2015). Mechanisms of muscle denervation in aging: insights from a mouse model of amyotrophic lateral sclerosis. *Aging Dis.* **6**, 380-389.
Patton, B. L., Cunningham, J. M., Thyboll, J., Kortesmaa, J., Westerblad, H., Edström, L., Tryggvason, K. and Sanes, J. R. (2001). Properly formed but improperly localized synaptic specializations in the absence of laminin alpha4. *Nat. Neurosci.* **4**, 597-604.
Prokop, A., Martín-Bermudo, M. D., Bate, M. and Brown, N. H. (1998). Absence of PS integrins or laminin A affects extracellular adhesion, but not intracellular assembly, of hemiadherens and neuromuscular junctions in Drosophila embryos. *Dev. Biol.* **196**, 58-76.
Rafuse, V. F., Polo-Parada, L. and Landmesser, L. T. (2000). Structural and functional alterations of neuromuscular junctions in NCAM-deficient mice. *J. Neurosci.* **20**, 6529-6539.
Rohrbough, J., Grotewiel, M. S., Davis, R. L. and Broadie, K. (2000). Integrin-mediated regulation of synaptic morphology, transmission, and plasticity. *J. Neurosci.* **20**, 6868-6878.
Rudolf, R., Khan, M. M., Labeit, S. and Deschenes, M. R. (2014). Degeneration of neuromuscular junction in age and dystrophy. *Front. Aging Neurosci.* **6**, 99.
Ruiz, R., Casañas, J. J., Südhof, T. C. and Tabares, L. (2008). Cysteine string protein-α is essential for the high calcium sensitivity of exocytosis in a vertebrate synapse. *Eur. J. Neurosci.* **27**, 3118-3131.
Samuel, M. A., Valdez, G., Tapia, J. C., Lichtman, J. W. and Sanes, J. R. (2012). Agrin and synaptic laminin are required to maintain adult neuromuscular junctions. *PLoS ONE* **7**, e46663.
Schulz, A. M., Jing, Z., Sánchez Caro, J. M., Wetzel, F., Dresbach, T., Strenzke, N., Wichmann, C. and Moser, T. (2014). Bassoon-disruption slows vesicle replenishment and induces homeostatic plasticity at a CNS synapse. *EMBO J.* **33**, 512-527.
Schwander, M., Shirasaki, R., Pfaff, S. L. and Müller, U. (2004). Beta1 integrins in muscle, but not in motor neurons, are required for skeletal muscle innervation. *J. Neurosci.* **24**, 8181-8191.
Singhal, N. and Martin, P. T. (2011). Role of extracellular matrix proteins and their receptors in the development of the vertebrate neuromuscular junction. *Dev. Neurobiol.* **71**, 982-1005.
Südhof, T. C. (2012). The presynaptic active zone. *Neuron* **75**, 11-25.
Truett, G. E., Heeger, P., Mynatt, R. L., Truett, A. A., Walker, J. A. and Warman, M. L. (2000). Preparation of PCR-quality mouse genomic DNA with hot sodium hydroxide and tris (HotSHOT). *BioTechniques* **29**, 52-54.
Tsai, P.-I., Wang, M., Kao, H.-H., Cheng, Y.-J., Lin, Y.-J., Chen, R.-H. and Chien, C.-T. (2012). Activity-dependent retrograde laminin A signaling regulates synapse growth at Drosophila neuromuscular junctions. *Proc. Natl. Acad. Sci. USA* **109**, 17699-17704.
Valdez, G., Tapia, J. C., Kang, H., Clemenson, G. D., Gage, F. H., Lichtman, J. W. and Sanes, J. R. (2010). Attenuation of age-related changes in mouse neuromuscular synapses by caloric restriction and exercise. *Proc. Natl. Acad. Sci. USA* **107**, 14863-14868.
Varoqueaux, F., Sons, M. S., Plomp, J. J. and Brose, N. (2005). Aberrant Morphology and Residual Transmitter Release at the Munc13-Deficient Mouse Neuromuscular Synapse. *Mol. Cell. Biol.* **25**, 5973-5984.
Vaux, D. L. (2012). Know when your numbers are significant. *Nature* **492**, 180-181.
Webster, R. G., Cossins, J., Lashley, D., Maxwell, S., Liu, W. W., Wickens, J. R., Martinez-Martinez, P., de Baets, M. and Beeson, D. (2013). A mouse model of the slow channel myasthenic syndrome: Neuromuscular physiology and effects of ephedrine treatment. *Exp. Neurol.* **248**, 286-298.
Yumoto, N., Kim, N. and Burden, S. J. (2012). Lrp4 is a retrograde signal for presynaptic differentiation at neuromuscular synapses. *Nature* **489**, 438-442.

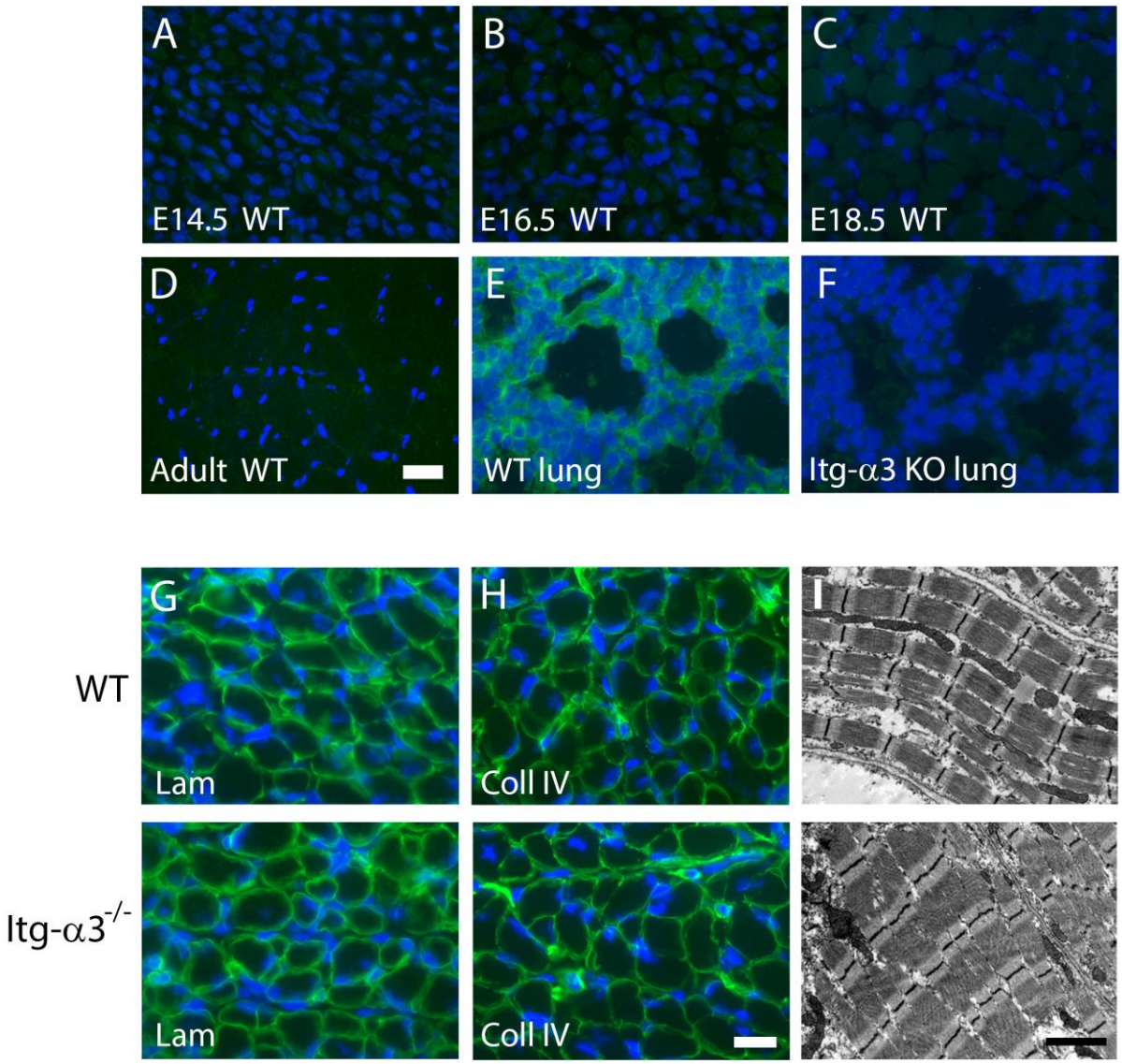

Fig S1. Integrin-α3 is not detectable in muscle by immunohistochemistry and has no major role in its development. Immunostaining for integrin-α3 (green) in transverse wild type intercostal muscle at multiple embryonic (A-C) and adult (D) stages. (E) Positive control tissue (wild type lung), and (F) negative control tissue (integrin-α3$^{-/-}$ lung), both at E18.5. (G, H) normal deposition of laminin (Lam) and collagen IV (Col IV), and normal myofibre morphology in transverse integrin-α3$^{-/-}$ muscle at E18.5. (I) normal organisation of myofibrils in wild type (top panels) and integrin-α3$^{-/-}$ (bottom panel) muscles, as examined by electron microscopy in longitudinal diaphragm at E18.5. Similar results observed in 3 animals/genotype for all. DAPI is shown in blue. Scale bars 20 μm (A-H), 2 μm (I).